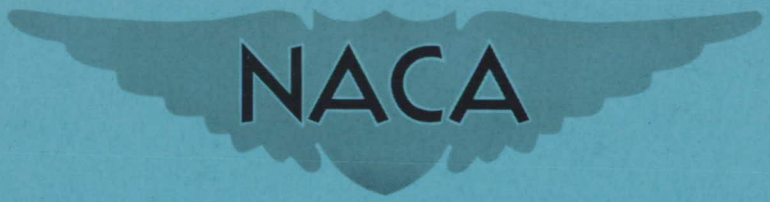

RESEARCH MEMORANDUM

INVESTIGATION OF THE DRAG OF BLUNT-NOSED BODIES OF REVOLUTION IN FREE FLIGHT AT MACH NUMBERS FROM 0.6 TO 2.3

By Harvey A. Wallskog and Roger G. Hart

Langley Aeronautical Laboratory
Langley Field, Va.

NATIONAL ADVISORY COMMITTEE
FOR AERONAUTICS

WASHINGTON
June 11, 1953
Declassified October 14, 1957

NACA RM L53D14a

NATIONAL ADVISORY COMMITTEE FOR AERONAUTICS

RESEARCH MEMORANDUM

INVESTIGATION OF THE DRAG OF BLUNT-NOSED BODIES OF REVOLUTION IN FREE FLIGHT AT MACH NUMBERS FROM 0.6 TO 2.3

By Harvey A. Wallskog and Roger G. Hart

SUMMARY

Fin-stabilized bodies of revolution with spherical, parabolic, flat, and conical noses, all with parabolic afterbodies, were tested with the rocket-model technique. The various nose shapes, which could provide suitable housings for guidance systems, were tested in free flight over a Mach number range from 0.6 to 2.3 and at Reynolds numbers, based on total body length, ranging from 10×10^6 to 80×10^6.

The drag data obtained in this investigation from models designed by replacing the original parabolic-nose point with various sized spherical segments indicate that small amounts of bluntness are beneficial over a limited range of low supersonic Mach numbers. Supersonic total drag coefficients are shown to increase markedly with larger degrees of bluntness. This rise in drag is shown to hold true, to varying degrees, for blunt noses with flat and conical surfaces placed at the apex. The increase in drag coefficient for a given size spherical nose is shown to be greater when the round nose replaces the tip of a higher fineness ratio parabolic nose. Calculated increments in drag coefficients due to rounding off a nose are compared with experimental results for a Mach number of 1.62.

INTRODUCTION

On the basis of previous experimental and theoretical investigations of fuselage drag at supersonic speeds, the nose shape for minimum drag coefficient is generally considered to be of high fineness ratio and tapered nearly to a point. In the design of an airplane or missile, a large departure from such a nose shape may incur a severe drag penalty with corresponding reductions in speed and range. For radar installations and optical seeker devices in airplanes and missiles, however, blunt noses may be the most satisfactory for "visibility." In order to help designers

make the necessary compromise, the Langley Pilotless Aircraft Research Division is investigating the drag of a number of nose shapes having desirable optical qualities. This investigation is being conducted at the Langley Pilotless Aircraft Research Station at Wallops Island, Va. with the use of rocket-propelled test vehicles. The results of other investigations of the drag of axially symmetric blunt-nosed shapes can be found in references 1 to 3 which present wind-tunnel data for several families of nose shapes. Drag data from nose shapes which may be suitable for the installation of optical seeker devices are presented in references 4 to 6, which show data for blunt noses modified to include spikes and windshields.

In references 7 and 8, drag data from rocket-propelled models were presented for several round-nosed bodies of revolution. The data presented herein supersedes that shown for the same configurations in these references. All the data of this report have been adjusted to include the effects of winds aloft on the measured model speed. The present results include data for additional round noses, for noses having blunt points, and for flat noses. All the configurations tested, with two exceptions, were designed by modifying the nose of a basic fin-body combination of nose fineness ratio 3.56 (total fineness ratio, 8.91). The data were obtained over a range of Mach number from 0.6 to 2.3 and Reynolds number based on body length, from 10×10^6 to 80×10^6.

SYMBOLS

r_x	body radius at station x, in.
x	distance along body axis from nose, in.
r_n	radius of spherical nose segment, in.
r_{max}	radius of body at station of maximum diameter, in.
r_n/r_{max}	nose radius ratio
L	body length, ft
n	fineness ratio, $\text{Length}/2r_{max}$
C_D	total drag coefficient based on body frontal area
W	model weight (after sustainer burnout), lb

g	acceleration due to gravity, ft/sec^2
a	model acceleration along flight path, ft/sec^2
γ	model flight-path angle measured from the horizontal, deg
ρ	air density, free stream, slugs/cu ft
S	body frontal area, sq ft
V	model air speed, ft/sec
V_c	speed of sound, free stream, ft/sec
M	Mach number, V/V_c
μ	absolute viscosity, free stream, slugs/ft-sec
R	Reynolds number, $\rho VL/\mu$

MODELS

A general view of each configuration tested appears in figure 1, equations of the profiles of the parabolic bodies are given in table I, and photographs of typical test vehicles are shown in figure 2. Each model was stabilized by three 45° sweptback fins located so that the trailing edges intersected the body at the 90.53 percent station of the unmodified configuration. For all configurations, the frontal area was 0.307 square foot, the base area was 0.0586 square foot, and the total exposed fin area was 1.69 square foot.

Modifications of The Body With Fineness Ratio 8.91

All but two of the configurations presented in this report were adapted from the parabolic configuration 6 of reference 9, which was a fin-stabilized body of revolution having a fineness ratio of 8.91 and the maximum diameter located at 40 percent of the body length. This body is herein designated configuration A.

Configurations B to I were designed by replacing the original nose point with various sized spherical segments. In each case the spherical segment and the unmodified portion of the body were tangent at the station where they met and the profile slope was continuous. Rearward of this tangent station, each configuration was identical to the basic body.

Four additional blunt-nosed bodies, adapted from configuration A, were tested. One flat-nosed body, configuration J, was designed by removing the spherical portion of configuration F $\left(r_n/r_{max} = 0.592\right)$. The second flat-nosed body L was designed by removing a portion of sphere H $\left(r_n/r_{max} = 0.806\right)$ so as to provide a flat surface of the same area as that of J. In order to provide another optically desirable nose shape, configuration K, a large-angle conical-nosed point was added to nose H $\left(r_n/r_{max} = 0.806\right)$ so that the conical surface just covered the flat surface of L and was tangent to the sphere and thus provided a continuous slope profile. Configuration N was designed by replacing the entire nose portion of the basic body (nose $n = 3.56$) with another parabolic nose of fineness ratio 2.

Modifications of the Body With Fineness Ratio 12.5

An additional round-nosed configuration (P, $r_n/r_{max} = 0.500$) was adapted from configuration 3 of reference 9, which also was a fin-stabilized body of revolution, but having a fineness ratio of 12.5 and the maximum diameter located at 60 percent of the body length (herein called configuration 0). Rearward of the maximum diameter location, the two basic parabolic bodies were nearly the same. The afterbody fineness ratio of configuration 0 was 5.0, whereas that of A was 5.35, and the fins were located at a common percentage of each total body length.

Model Construction and Finish

All models were made of laminated wood, sanded and finished to form a smooth and fair surface. Figures 2(a) and (b) illustrate the two materials used to finish the model surface. The first model is typical of those models finished with clear lacquer which attained a maximum Mach number of about 1.5. The second photograph shows a model, finished with Phenoplast, which was typical of those reaching maximum Mach numbers of about 2.3. Phenoplast, a phenolic-resin lacquer, is a commercial preparation which is better able to withstand the more severe aerodynamic heating associated with the higher Mach number. The fins were polished duralumin.

TESTS AND METHODS

Rocket-Model Technique

Each model was launched from the ground and accelerated to supersonic speeds by means of a two-stage propulsion system. For the lower speed models (maximum $M \approx 1.5$), the first stage or booster was a 5-inch HVAR motor. For the higher speed models (maximum $M \approx 2.3$), the booster was a 6-inch ABL Deacon rocket motor. For all models, the second stage or sustainer was a 3.25-inch Mk 7 rocket motor. Figures 2(c) and (d) illustrate the two propulsion arrangements used.

Each booster was equipped with four stabilizing fins and engaged the model through a nozzle-plug adapter. The rate of divergence of the booster from the model flight path, after booster separation, was increased by the use of canard flaps on the booster for the low-speed cases and dynamic pressure actuated flaps for the high-speed cases. All models were launched at an elevation angle of approximately 65° from the horizontal.

Total-drag data were obtained for each model in its coasting flight. After sustainer burnout, the only forces acting on a model along its free-flight path were drag and a component of weight. Relating the sum of these forces to the model deceleration and solving for drag coefficient yields the equation

$$C_D = \frac{2W(-a - g \sin \gamma)}{g\rho V^2 S}$$

Thus, in order to determine the total drag coefficients for such a model, it is necessary to measure the quantities a, V, ρ, and γ, which vary continually during the flight.

Instrumentation

The instrumentation used to obtain drag data for these nontelemetered models consisted of a CW Doppler radar set, an NACA modified SCR 584 radar set, and radiosonde units. The CW Doppler radar set produces an oscillating trace on a film which is accurately marked for time intervals. The frequency of the cycles indicates the radial velocity of the model relative to two stationary antennas which are placed within a few feet of the launching site. The SCR 584 radar set, located about 1300 feet to the

rear of the launching site, records a time history of the model location expressed in spherical coordinates. Immediately after firing, a radiosonde is released. This unit transmits values of atmospheric pressure and temperature from which the variations of density, viscosity, and velocity of sound with altitude are determined.

Space-location time histories of radiosonde balloons are obtained from the SCR 584 radar set. From these data are obtained the variation of wind speed and direction with altitude. For most of the results presented in this paper, however, winds-aloft data by direct measurement were not available and, therefore, were estimated for the Wallops Island test range by the Meteorology Section of the Langley Flight Research Division from information recorded at nearby weather stations. By means of these winds-aloft data, the measured model ground speeds were then adjusted to airspeeds.

Data Reduction

The two radar records, space location and speed, are related to each other by the time element, and radiosonde data are connected to both through altitude. The SCR 584 radar data are converted from spherical coordinates to altitude and horizontal range from the launching site. With the flight-path time history thus determined, trigonometric corrections are applied to the CW Doppler radar data to convert radial velocity to tangential velocity along the flight path. At this stage the component of the wind vector (either measured or estimated) in the flight-path direction is added to the measured model ground speed and model airspeed is obtained. The model acceleration along the flight path is obtained by numerical differentiation of the tangential velocity. Mach numbers and Reynolds numbers are computed from a combination of the radar and radiosonde data.

The Reynolds numbers obtained in flight and plotted against Mach number in figure 3 include all those for models of each configuration where more than one was flown. The flight tests covered a range of body-length Reynolds numbers from 10×10^6 to 80×10^6 and Mach numbers from 0.6 to 2.3.

Probable Errors

The two main sources of error in the determination of drag coefficient against Mach number curves are (1) inaccuracies in the instruments and in the reduction of instrument recorded data and, (2) errors in the determination of winds-aloft data.

A probable error due to the first source has been obtained by a consideration of instrument accuracy and of the probable error involved in the data-reduction system. The contribution of the second source to the total probable error was evaluated by comparing actual measured winds aloft over the test range with estimates made by the Meteorology Section based on other available wind data.

The probable error in the faired curves of total drag coefficient against Mach number presented in this paper is believed to be less than ±0.008 in drag coefficient and ±0.010 in Mach number. Figure 4 illustrates the type of agreement in drag coefficient and Mach number obtained for flights of identical models.

RESULTS AND DISCUSSION

Spherical Bluntness

Total-drag data for the round-nosed configurations are shown in figure 5(a) for Mach numbers up to 1.5 and the curves of the four higher-speed models are repeated in figure 5(b) for Mach numbers up to 2.3. For models having nose radius ratios of 0.500 and greater, the drag coefficients increased with increasing Mach number over the entire supersonic range of the tests. For models having nose radius ratios of 0.187, 0.274, and 0.387, the drag coefficients were nearly constant at the highest Mach number reached by the respective models in contrast with the drag coefficients of the pointed-nosed, basic body, which decreased after reaching a maximum at Mach number 1.2. Rounding off the nose to radius ratios of 0.187 and 0.274 caused the supersonic drag to be lower than that of the pointed body up to a Mach number of 1.4. The reduction for both bodies at Mach numbers around 1.2 amounted to about 4 percent. At Mach numbers between 1.0 and 1.1, rounding off the nose to even larger radii (to $r_n/r_{max} = 0.5$) appears to have produced no increase in drag. The trends of the subsonic data indicate that bluntness may have little effect on the total drag at low subsonic speeds.

In figure 6(a) the differences between the total drag coefficients of the round-nosed bodies and those of the basic body are plotted against nose radius ratio for several supersonic Mach numbers. A similar cross plot for Mach number 1.62 is compared in figure 6(b) with a calculated curve which neglects the effects that rounding off the nose may have on the flow over the unmodified portion of the body. In calculating the drag increments, interferometer data from reference 10 were used to obtain the pressure drag of the spherical segments; linearized theory (ref. 11) was used to allow for the pressure drag of the replaced nose points; and a viscous skin-friction drag coefficient of 0.0023 was assumed to act

over the wetted areas of the added and replaced nose portions. Since the calculated curve shows a continual rise in drag with increasing bluntness, it appears that the reductions in total drag noted for smaller radius ratios are due to interference effects.

Favorable interference between the spherical and parabolic parts of the noses might be anticipated from the interferometer data, which indicate that the pressures at the junctures or tangent points are far lower than those predicted by linearized theory for corresponding points on the unmodified body. The crossing of the two curves in figure 6(b) followed by an interval of unfavorable interference at high radius ratios might likewise be anticipated, since, for a value of $r_n/r_{max} = 1.00$, low pressures from the hemisphere would act on the negatively sloping surfaces of the afterbody and thus increase the drag. The presence of this same effect at high subsonic speeds may account for the early drag rise shown by configuration I ($r_n/r_{max} = 1.0$) in figure 5(a). Pressure-distribution data of reference 12, at a Mach number of 0.9, show that large negative pressures generated by flow around a large hemispherical nose are present on a negatively sloping afterbody.

Figure 7 shows a comparison of the effects of rounding off the two basic bodies of fineness ratios 8.91 and 12.5 to a nose radius ratio of 0.500. Since the fins and afterbody fineness ratios were approximately the same for the two basic configurations, almost all the original difference in drag was due to the effects of nose fineness ratio. The drag increment due to rounding off the higher fineness ratio nose was considerably larger than that obtained for the lower fineness ratio nose and the two round-nosed bodies had about the same drag. Nose fineness ratio, therefore, appears to have little effect on the drag of bodies having noses with appreciable degrees of bluntness.

Also shown in figure 7 are the calculated drag-coefficient increments at Mach number 1.62 due to rounding off the two noses. The increment shown for the change from configurations A to E was obtained from figure 6(b). The increment due to rounding off the higher fineness ratio basic body 0 was calculated by the same method. Both calculated increments are too large, although that for the higher fineness ratio body appears to be somewhat closer to the measured increment.

On the basis of experimental pressure distributions (ref. 13) and theoretical considerations (ref. 14), it is possible to describe qualitatively the flow about a blunt, axially symmetric body traveling at supersonic speeds. The body is preceded by a curved, detached shock wave which is normal to the flow at the axis of symmetry and approaches the free-stream Mach angle asymptotically at large distances from the body. In the region of the body apex the flow is subsonic and local stagnation conditions are reached at the apex itself. Moving rearward,

the flow undergoes a rapid expansion and becomes supersonic. The flow may then continue to accelerate and expand and as a result reaches pressures well below those encountered on pointed noses of smooth profile. Such pressures acting on a positively sloping part of the nose provide a negative contribution to total body drag and they tend to offset the effect of the high pressures acting near the blunt apex. The present data for spherical bluntness indicate that, in cases where the low pressures had a sufficiently large part of the nose frontal area on which to act, their effect on total drag was of the same order as that of the apex pressures, and resulted in little change in total drag coefficient. Similar results are reported in reference 15 for a wind-tunnel investigation in which round-nosed bodies were tested at Mach numbers up to 7.4.

Other Kinds of Bluntness

Figures 8 to 10 show drag comparisons for various blunt-nosed shapes. The data will be discussed in the light of certain approximations suggested by Moeckel in reference 13. According to these approximations, the flow about a blunt body of revolution first becomes supersonic at that station on the nose where the profile slope is equal to that of the bluntest cone to which a shock wave can attach. Such a criterion is applied to convex-body profiles with continuous slopes. If there is a convex corner at some station ahead of the "attachment slope" station, however, the flow around the corner will become supersonic and may or may not shock back to subsonic speeds. Other assumptions of reference 13 lead to the result that the mean pressure coefficient over the subsonic portion of the nose frontal area is independent of the profile shape and a function of free-stream Mach number alone.

Figure 8 shows a comparison of four noses having fineness ratios of about 2. Configuration L was designed by removing the front part of the round-nosed body H so as to form a flat surface at the apex. Configuration K was designed by adding a blunt tangent cone to the front of H. Both modifications of configuration H lie forward of the attachment slope stations for the Mach number range of the tests. Adding the tangent cone had only a small effect on the supersonic drag of the round-nosed configuration, as might be expected on the basis of Moeckel's assumptions. The lower drag of configuration L may have been caused by the sonic point moving forward to the corner; this movement confines the subsonic part of the flow with its higher pressures to a smaller portion of the frontal area.

At Mach numbers above 2.5, when the shock is attached to the cone, adding the tangent cone might be expected to lower the drag of the round-nosed configuration. Likewise, at higher speeds, flattening the nose may

increase the drag since, according to Moeckel's assumptions, the supersonic part of the flow on the round nose would continue to move forward with increasing Mach number, whereas the flow over the entire flat surface would remain subsonic.

Included in figure 8 for the purposes of comparison are drag data for a body which was designed by replacing the entire $n = 3.56$ parabolic nose with another parabolic nose of $n = 2$. This figure illustrates the large reductions in supersonic drag which may be obtained for a given nose fineness ratio if a blunt apex is not required for visibility.

In figure 9, drag data for the round-nosed configuration F are compared with those for configuration J designed by removing the spherical part of F so as to form a flat surface at the apex. In contrast with the results of figure 8, flattening the nose here increased the supersonic drag. In this case, however, the spherical segment was entirely removed. Thus, according to Moeckel's assumptions, the station at which the flow became supersonic was moved rearward to the corner. The drag increase for J would then be due to the high-pressure subsonic part of the flow occupying a larger portion of the frontal area.

Drag data for the two flat-nosed bodies are compared in figure 10. Since the flat surfaces are of equal area, this comparison illustrates the differences in drag which may exist between two noses that satisfy the same optical requirements. The lower supersonic drag of configuration L may have been due to its higher profile slope in the region just behind the corner, since the low pressures which followed the expansion at the corner were thus provided with a greater portion of the frontal area on which to act before recovering.

CONCLUSIONS

Fifteen different fin-stabilized bodies of revolution were flown (eleven configurations up to a Mach number of about 1.5 and four up to a Mach number of about 2) in order to determine some effects of nose bluntness on the drag of basically parabolic bodies. The original nose points of the two parabolic bodies with different nose fineness ratios were modified to include several degrees of spherical bluntness and also flat surfaces and a blunt cone at the apex. The following effects were noted:

1. Small degrees of spherical bluntness on parabolic noses produced decreases in total drag coefficients for the Mach number range from 1.0 to about 1.4. For example, a value of the nose radius ratio of r_n/r_{max} of approximately 0.2 produced about a 4-percent reduction in drag from that of the basic body at a Mach number of 1.2.

2. Larger degrees of spherical bluntness up to $r_n/r_{max} \approx 0.5$ did not produce an increase in drag coefficient for Mach numbers up to 1.1. However, noses having values of $r_n/r_{max} = 0.5$ and greater showed drag coefficients increasing with Mach number over the entire supersonic range of the tests.

3. Nose fineness ratio appeared to have little effect on the total drag coefficients of bodies having noses with appreciable degrees of spherical bluntness. For example, a round nose of $r_n/r_{max} = 0.5$ added to parabolic noses of fineness ratios of approximately 3.5 and 7.5 produced nearly the same total drag coefficients at low supersonic speeds.

4. When, on a round-nosed body, a portion of the spherical nose was removed so that a flat surface was formed at the apex, a reduction in total drag was realized at supersonic speeds. When the entire spherical part of the nose was removed, however, a large increase in drag was observed.

5. Adding a blunt tangent cone to a round-nosed model so as to cover only a portion of the spherical nose produced a small decrease in drag coefficient at supersonic speeds.

6. When the nose of a parabolic body is modified to incorporate a relatively large spherical nose, the increase in drag due to this modification can be estimated by the use of existing experimental data and theoretical techniques. Calculated values of drag-coefficient increment, at a Mach number of 1.62, agreed well with experimental results for values of $r_n/r_{max} \approx 0.8$ to 1.0.

Langley Aeronautical Laboratory,
National Advisory Committee for Aeronautics,
Langley Field, Va.

REFERENCES

1. Perkins, Edward W., and Jorgensen, Leland H.: Investigation of the Drag of Various Axially Symmetric Nose Shapes of Fineness Ratio 3 for Mach Numbers From 1.24 to 3.67. NACA RM A52H28, 1952.

2. DeLeo, R. V., and Akerman, John D.: The Effect of Nose Shape on Missile Nose Drag. Res. Rep. 55, Univ. Minn., Inst. Tech., Feb. 15, 1950.

3. Linstone, Harold A.: Sphere-Tipped Nose Shapes in Axially Symmetric Supersonic Flow. TM No. 289, Hughes Aircraft Co., Mar. 15, 1952.

4. Piland, Robert O.: Preliminary Free-Flight Investigation of the Zero-Lift Drag Penalties of Several Missile Nose Shapes for Infrared Seeking Devices. NACA RM L52F23, 1952.

5. Beastall, D., and Turner, J.: The Effect of a Spike Protruding in Front of a Bluff Body at Supersonic Speeds. TN No. Aero. 2137, British R.A.E., Jan. 1952.

6. Alexander, Sidney R.: Flight Investigations at Low Supersonic Speeds To Determine the Effectiveness of Cones and a Wedge in Reducing the Drag of Round-Nose Bodies and Airfoils. NACA RM L8L07a, 1949.

7. Hart, Roger G.: Flight Investigation of the Drag of Round-Nosed Bodies of Revolution at Mach Numbers From 0.6 to 1.5 Using Rocket-Propelled Test Vehicles. NACA RM L51E25, 1951.

8. Hart, Roger G.: Flight Investigation at Mach Numbers From 0.8 to 1.5 To Determine the Effects of Nose Bluntness on the Total-Drag of Two Fin-Stabilized Bodies of Revolution. NACA RM L50I08a, 1950.

9. Hart, Roger G., and Katz, Ellis R.: Flight Investigations at High-Subsonic, Transonic, and Supersonic Speeds To Determine Zero-Lift Drag of Fin-Stabilized Bodies of Revolution Having Fineness Ratios of 12.5, 8.91, and 6.04 and Varying Positions of Maximum Diameter. NACA RM L9I30, 1949.

10. Gooderum, Paul B., and Wood, George P.: Density Fields Around a Sphere at Mach Numbers 1.30 and 1.62. NACA TN 2173, 1950.

11. Jones, Robert T., and Margolis, Kenneth: Flow Over a Slender Body of Revolution at Supersonic Velocities. NACA TN 1081, 1946.

12. Cole, Richard I.: Pressure Distributions on Bodies of Revolution at Subsonic and Transonic Speeds. NACA RM L52D30, 1952.

13. Moeckel, W. E.: Experimental Investigation of Supersonic Flow With Detached Shock Waves for Mach Numbers Between 1.8 and 2.9. NACA RM E50D05, 1950.

14. Busemann, Adolf: A Review of Analytical Methods for the Treatment of Flows With Detached Shocks. NACA TN 1858, 1949.

15. Sommer, Simon C., and Stark, James A.: The Effect of Bluntness on the Drag of Spherical-Tipped Truncated Cones of Fineness Ratio 3 at Mach Numbers 1.2 to 7.4. NACA RM A52B13, 1952.

TABLE I

EQUATIONS OF THE PARABOLIC ARCS DEFINING THE BASIC CONFIGURATIONS

Configuration	r_x, in.	
	Forebody profile	Afterbody profile
A	$0.2807x - 0.005251x^2$	$2.812 + 0.07018x - 0.001313x^2$
[a]N	$-8.149 + 0.8907x - 0.01667x^2$	$2.812 + 0.07018x - 0.001313x^2$
O	$0.1334x - 0.001186x^2$	$-0.9962 + 0.1688x - 0.001501x^2$

[a]Coordinates given from O station of A.

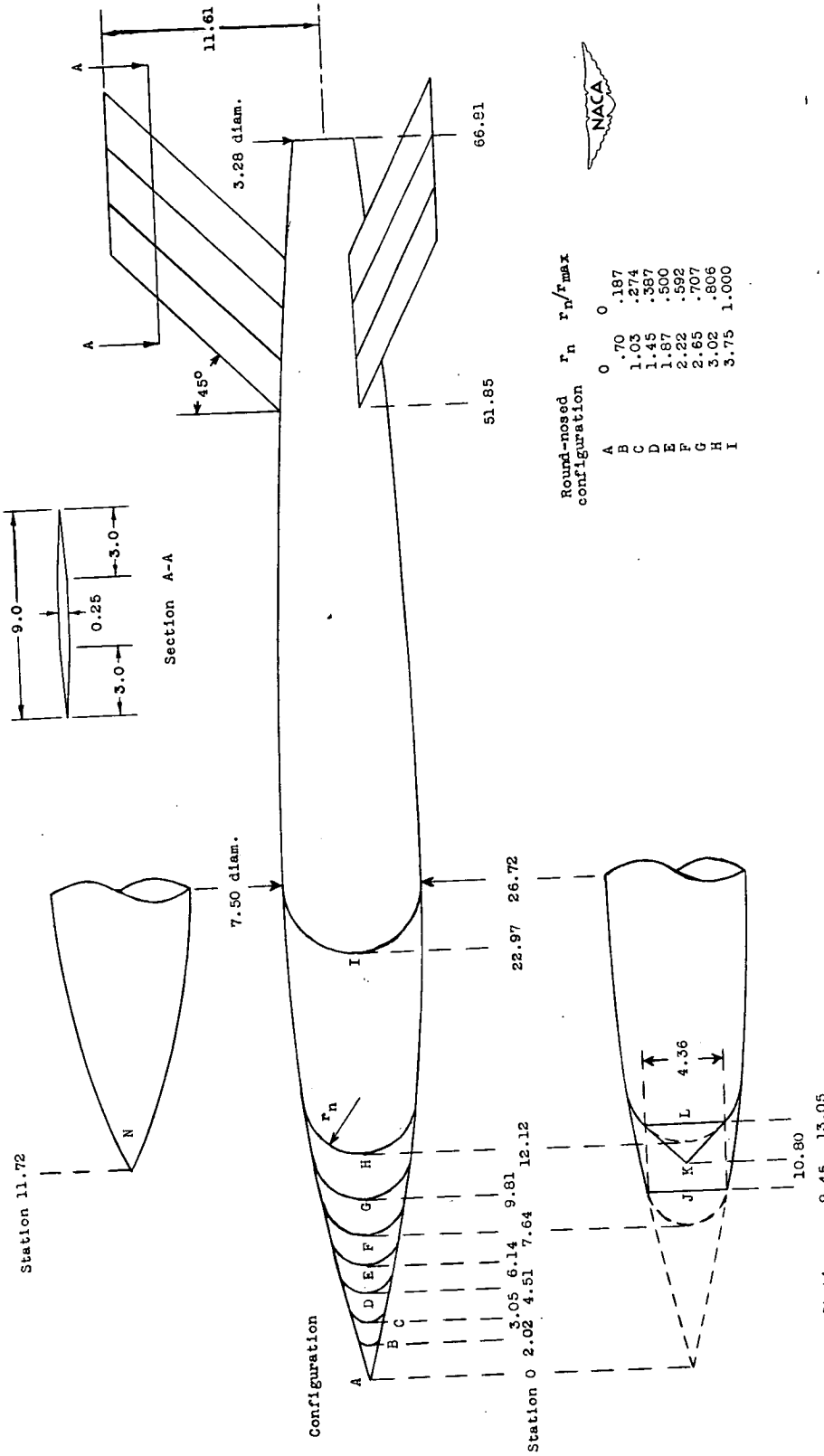

(a) Basic-body, fineness ratio, 8.91.

Figure 1.- General view of test configurations. Dimensions are in inches.

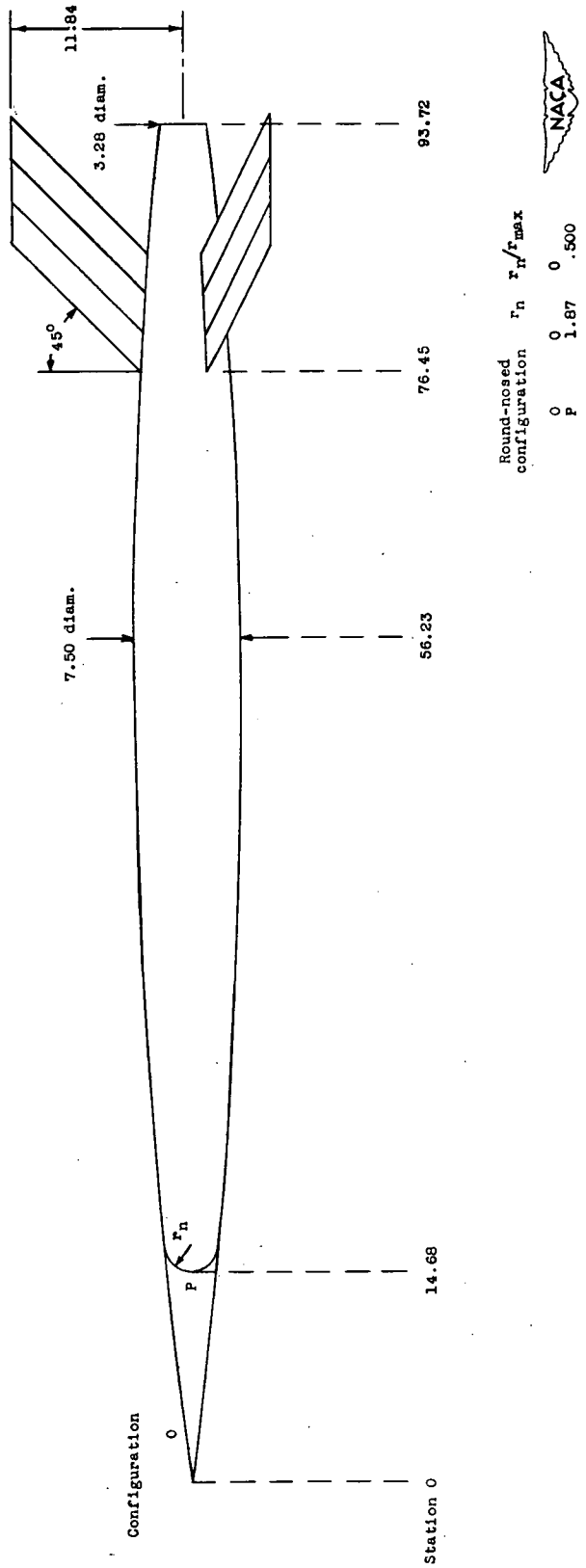

(b) Basic-body fineness ratio, 12.5.

Figure 1.- Concluded.

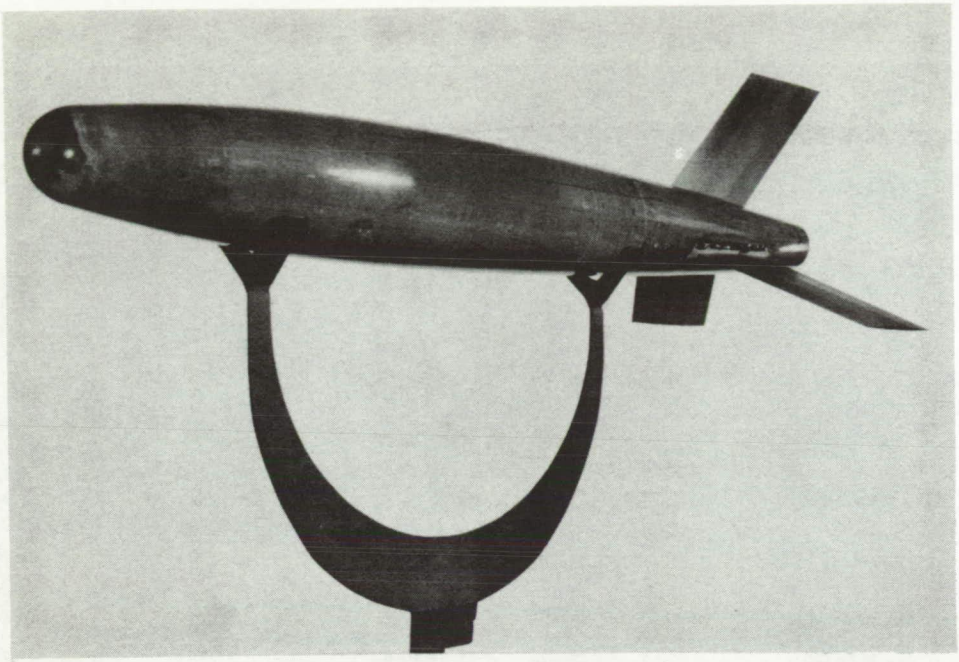

(a) Configuration F. L-69369.1

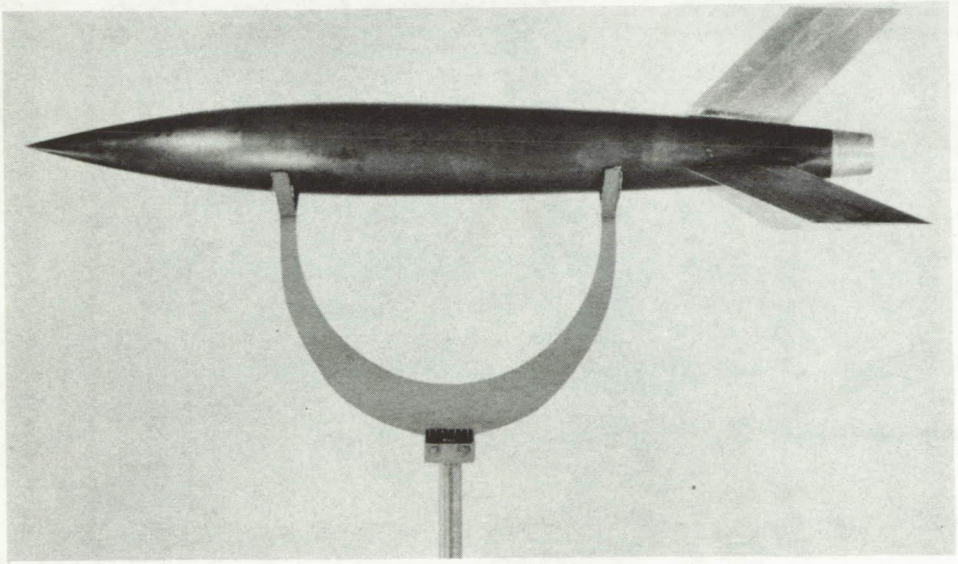

(b) Configuration A. L-71983.1

Figure 2.- Typical test vehicles and launching arrangements.

(c) Configuration G on launcher.

Figure 2.- Continued.

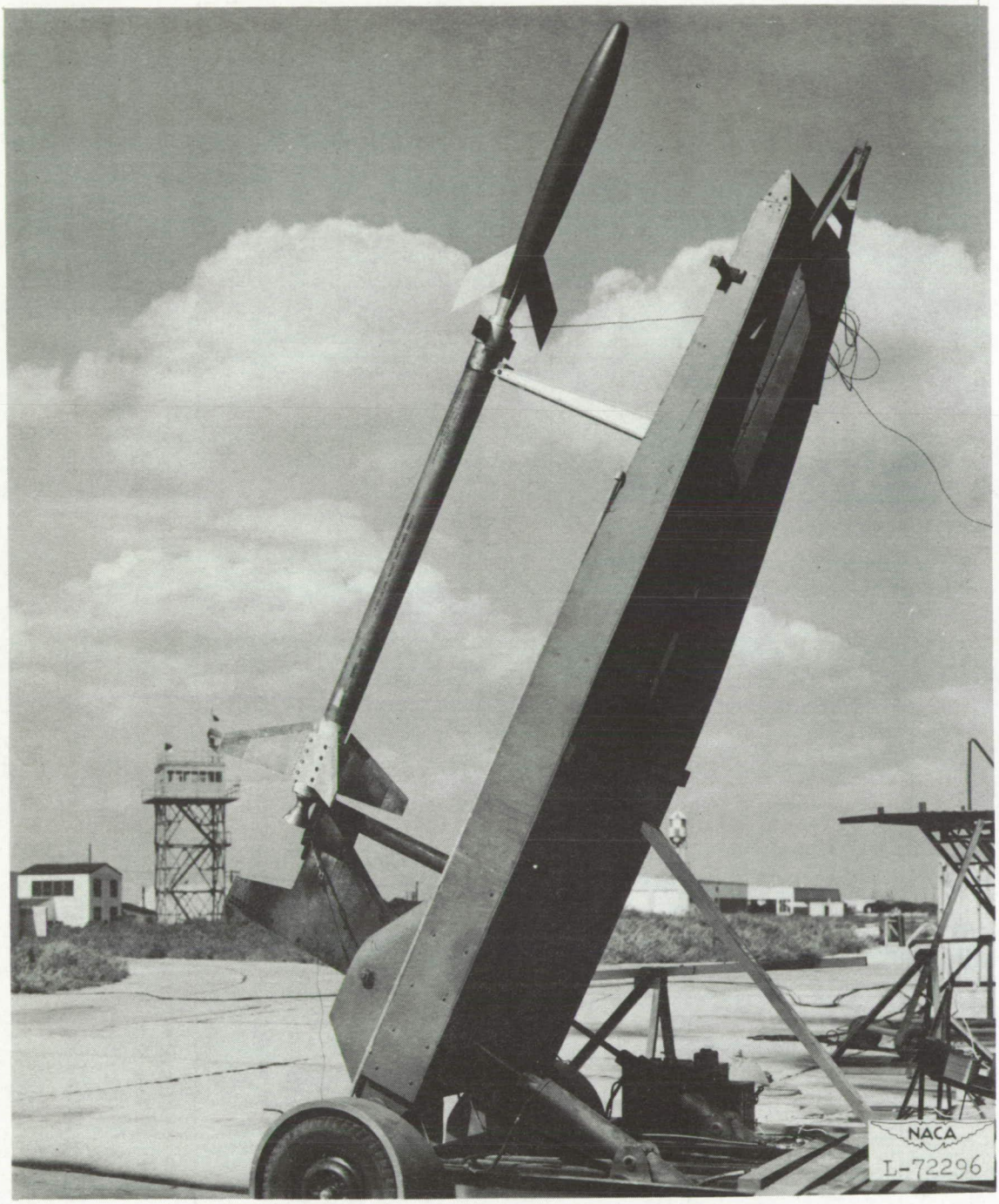

(d) Configuration E on launcher.

Figure 2.- Concluded.

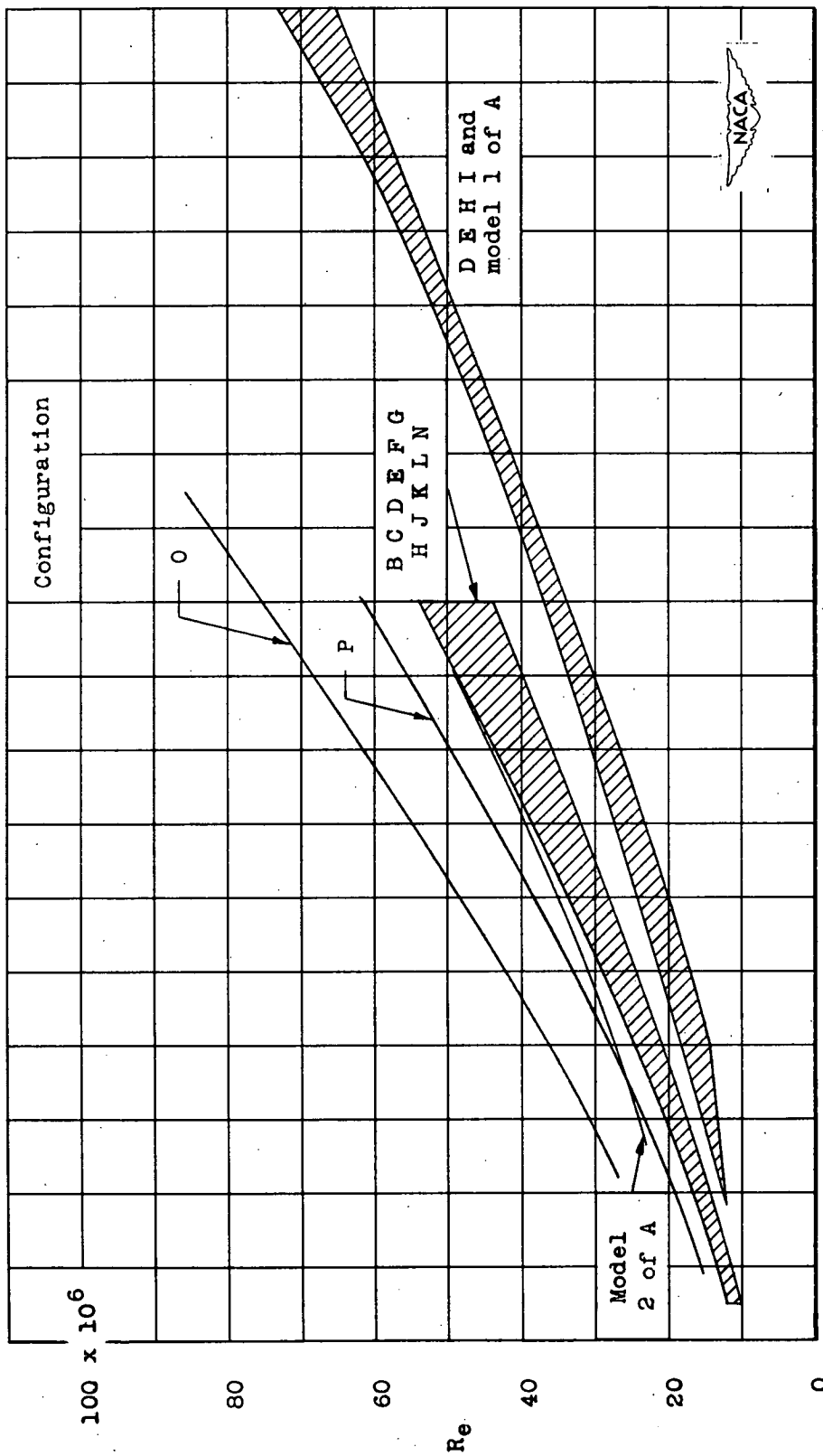

Figure 3.- Reynolds number, based on body length, against Mach number for the present configurations and for configurations from references 7 to 9.

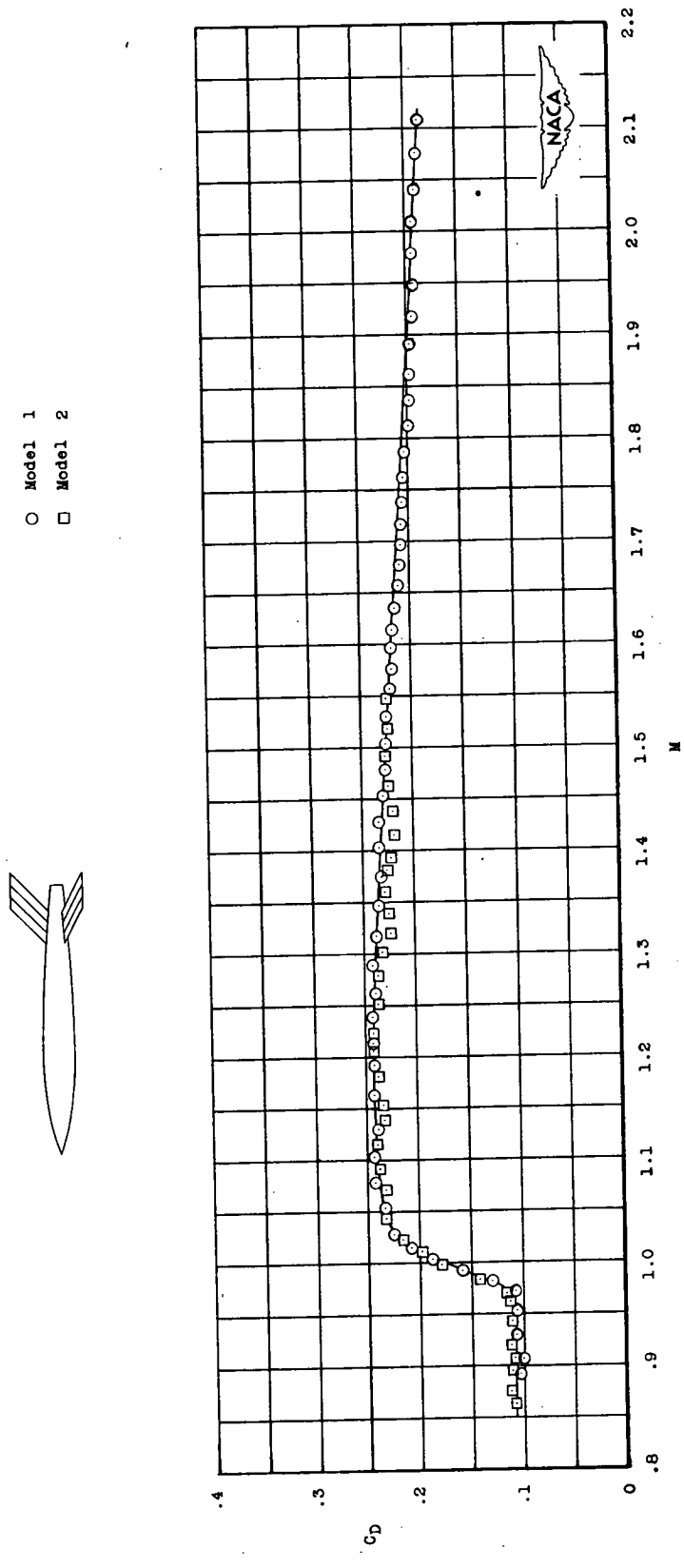

Figure 4.- Drag coefficient against Mach number for the two models of configuration A. Fineness ratio, 8.91.

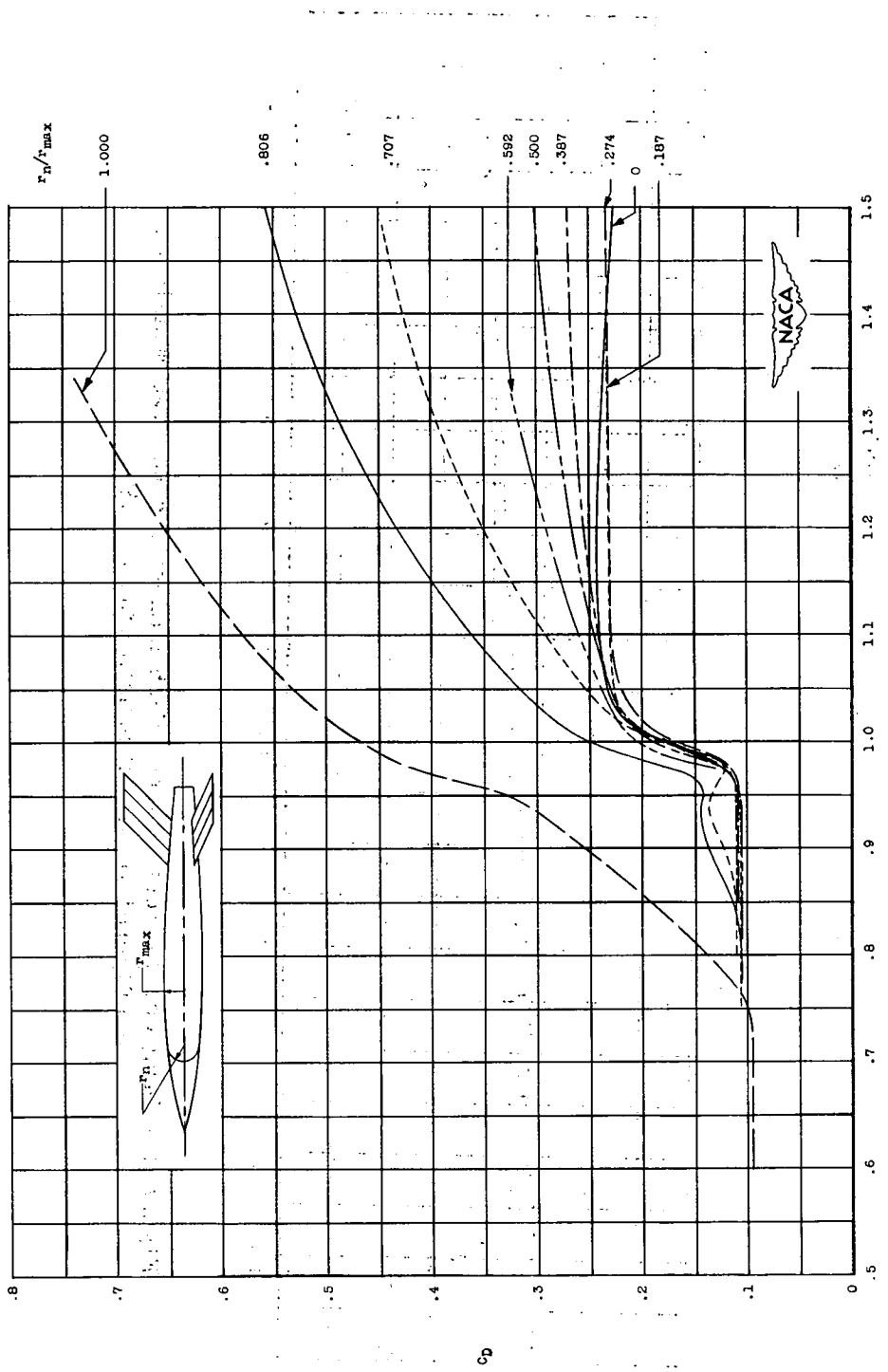

(a) All round-nosed models.

Figure 5.- Drag coefficient against Mach number for configurations obtained by rounding off the nose of the basic body of fineness ratio 8.91. (Configurations A to I).

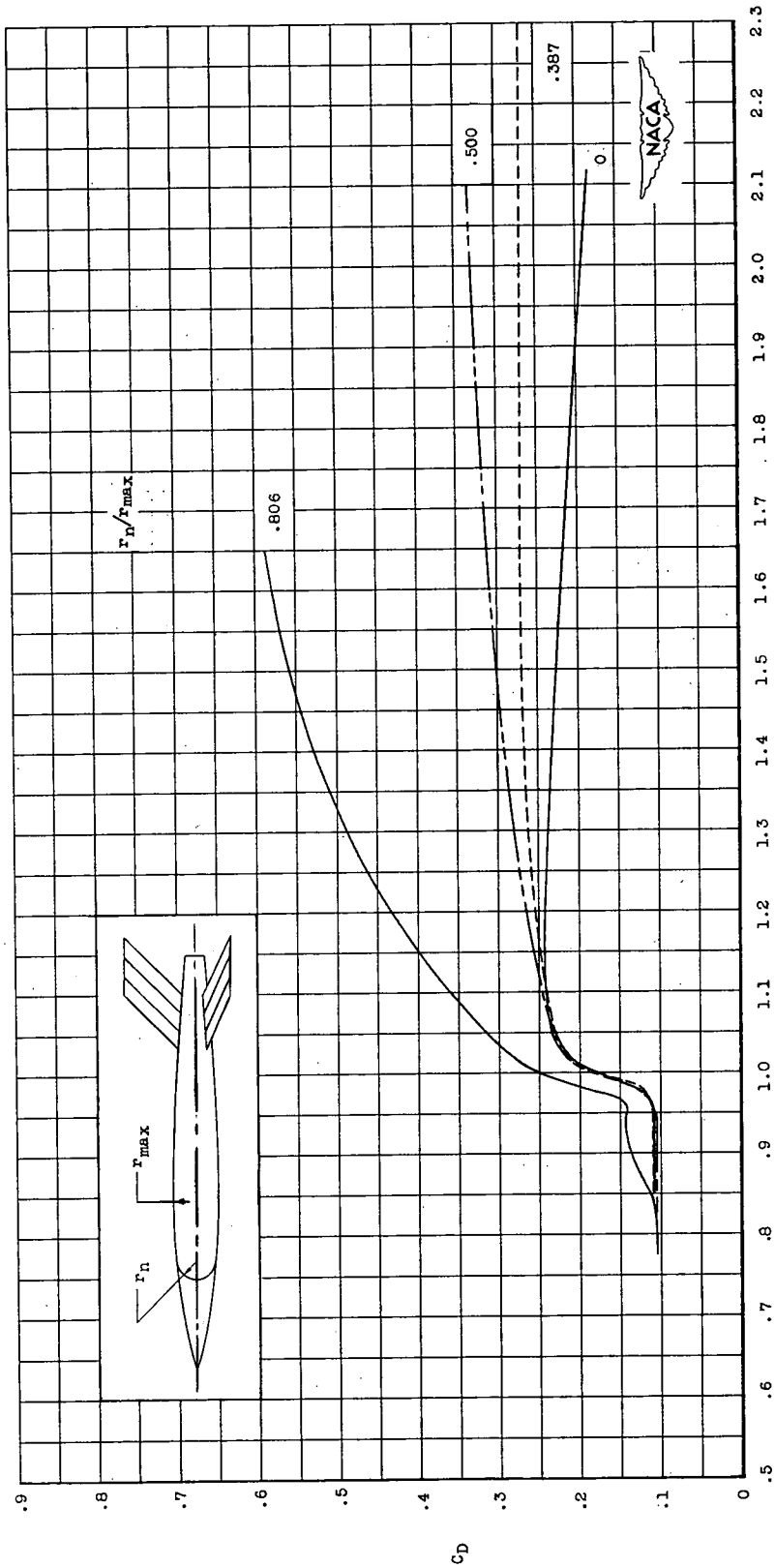

(b) High Mach number series.

Figure 5.- Concluded.

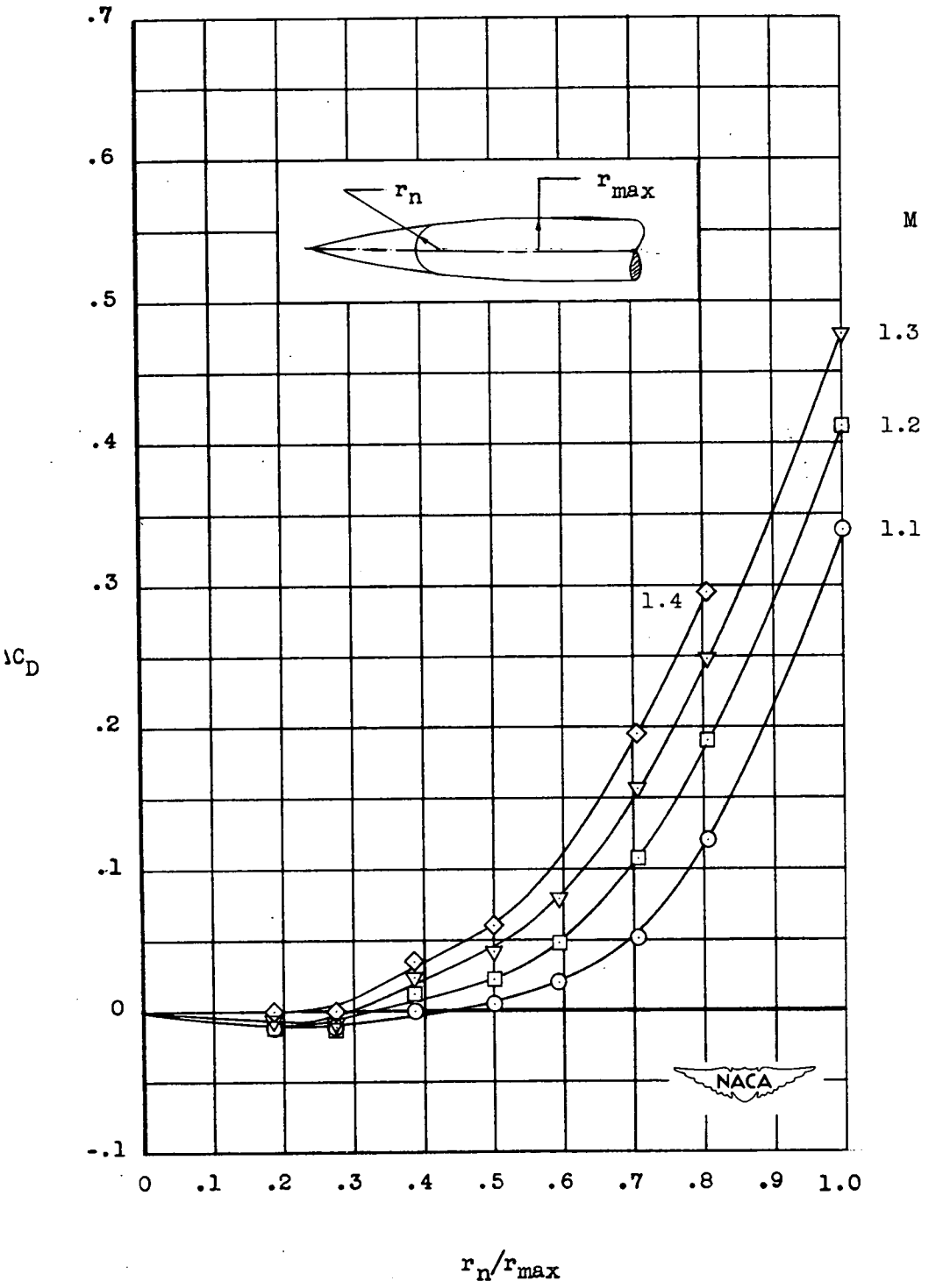

(a) Mach numbers 1.1 to 1.4.

Figure 6.- Drag-coefficient increments due to rounding off a nose. Basic-body fineness ratio, 8.91.

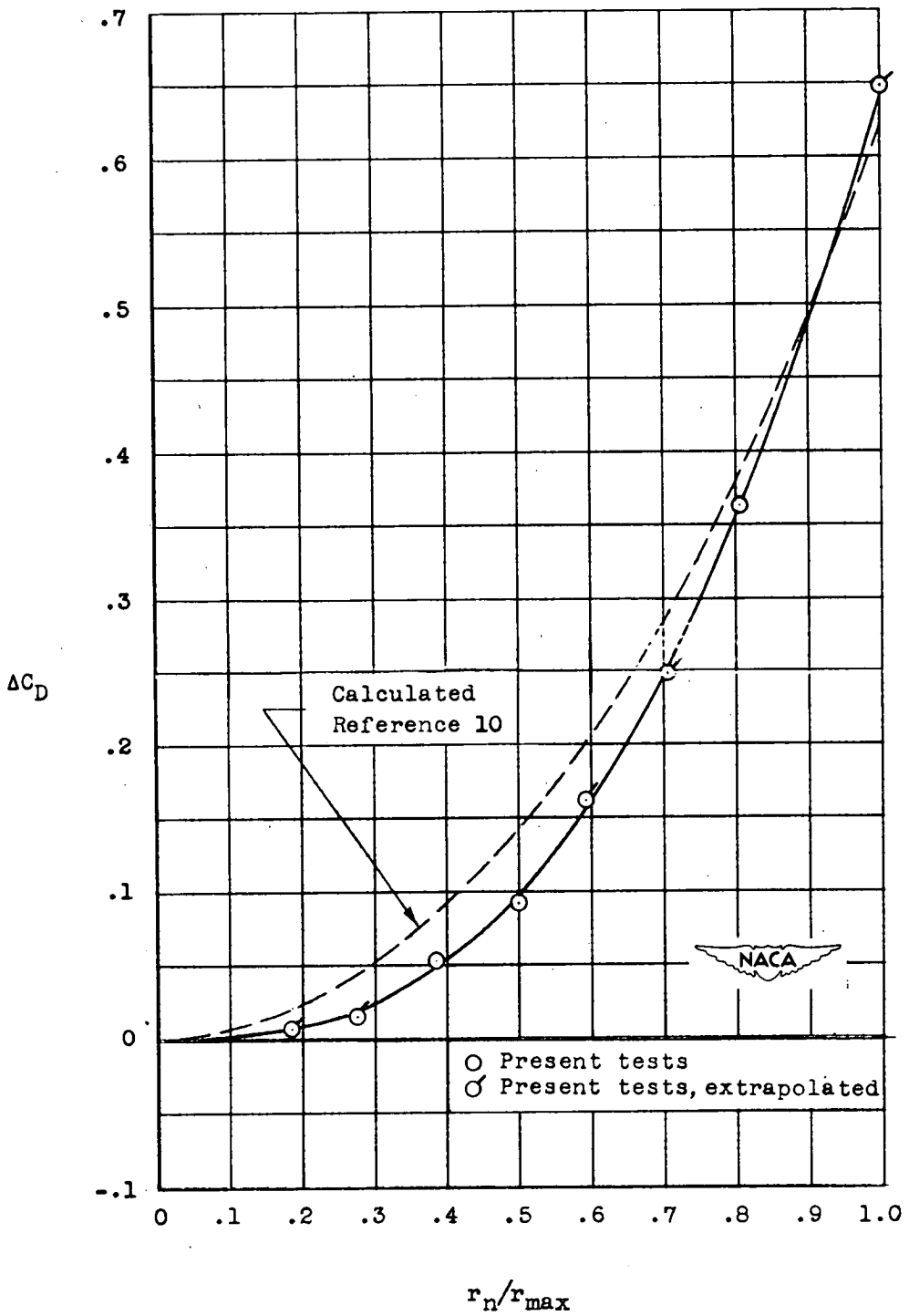

) Comparison of drag-coefficient increments with those estimated from sphere data at Mach number 1.62.

Figure 6.- Concluded.

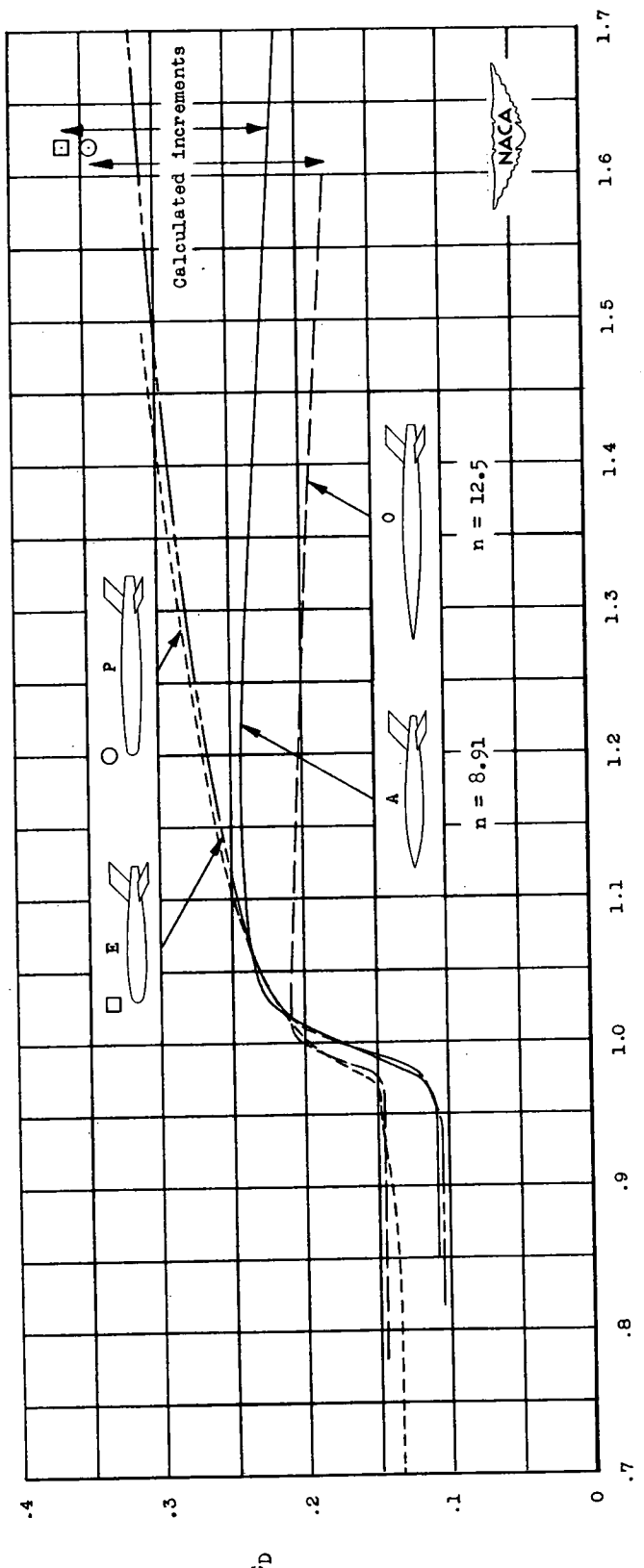

Figure 7.- Drag effects of rounding off two bodies to a nose radius ratio of 0.500.

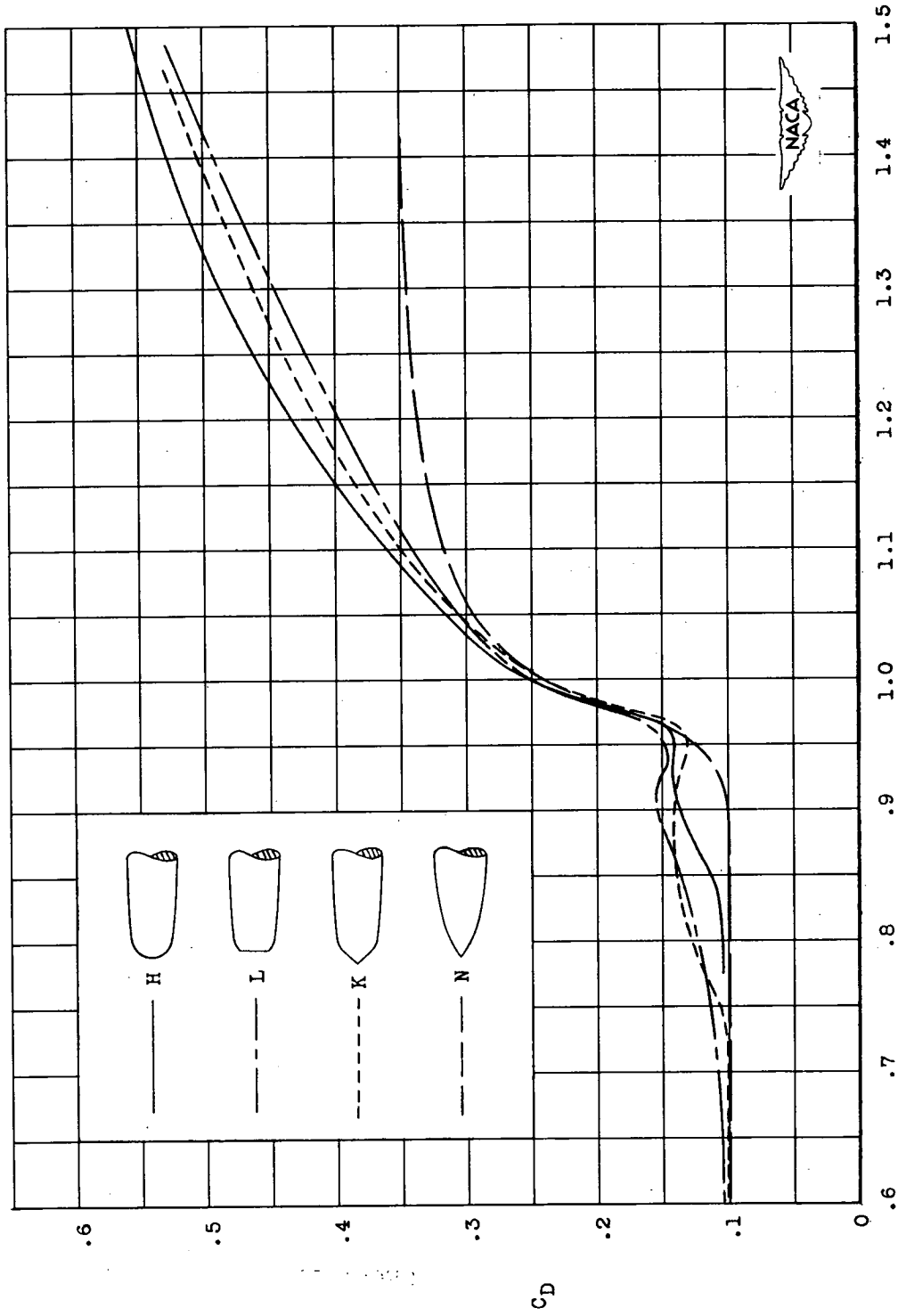

Figure 8.- Comparison of drag coefficient for four configurations with nose fineness ratio about 2.

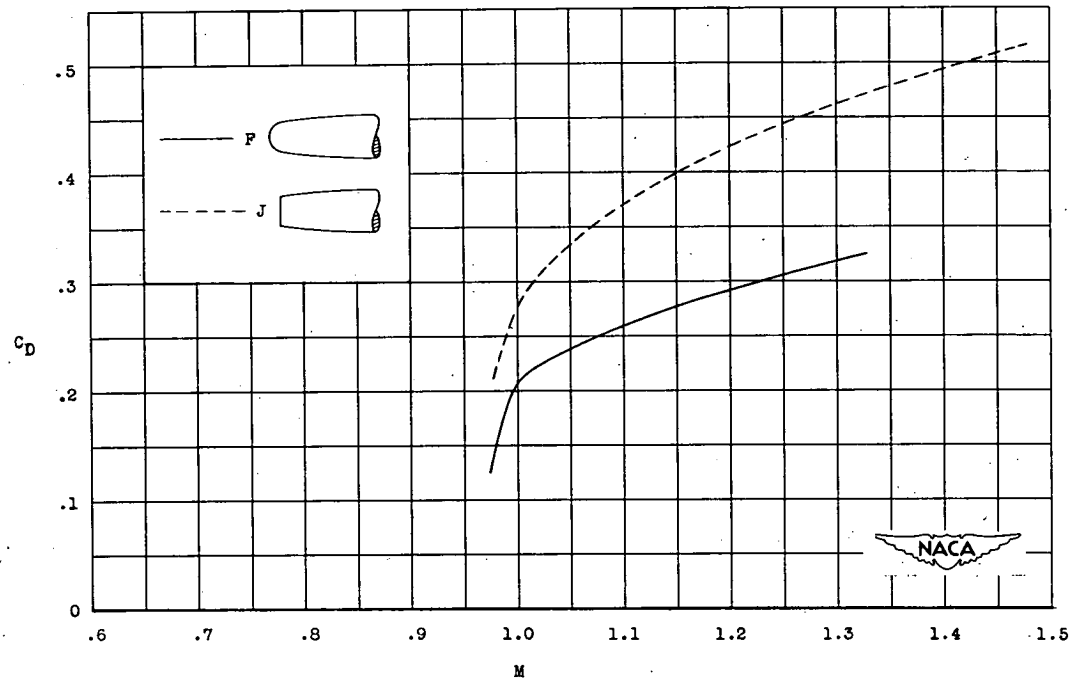

Figure 9.- The effects on drag coefficient of adding a spherical segment to a flat-nosed configuration.

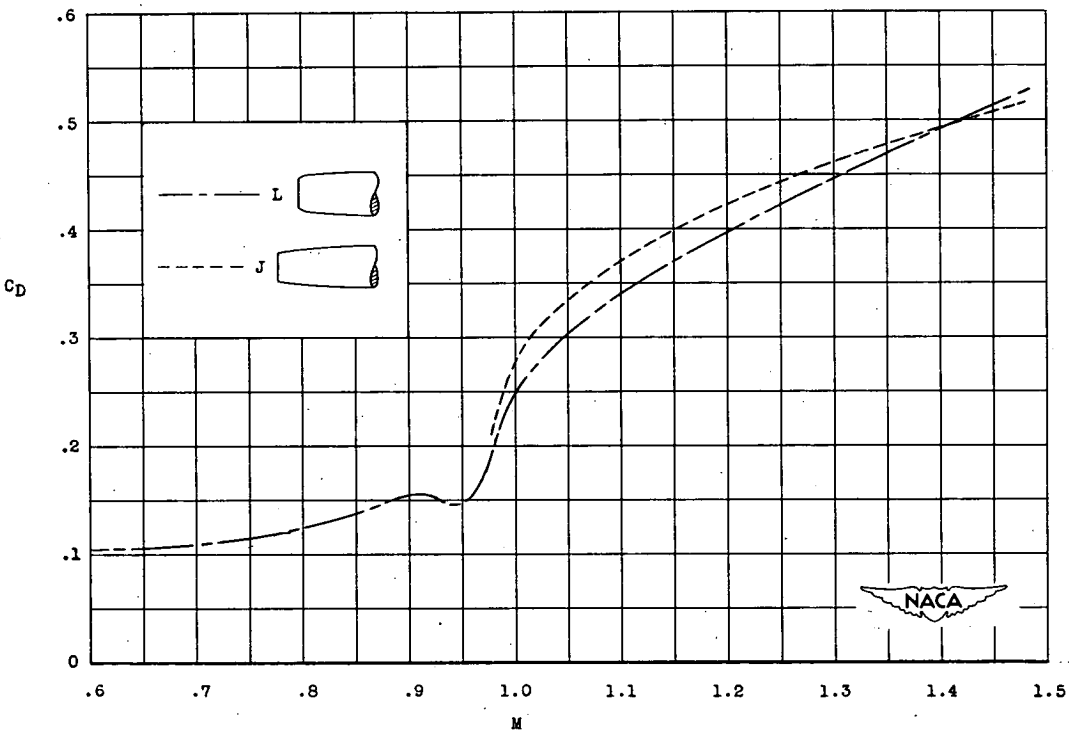

Figure 10.- Drag coefficient against Mach number for the flat-nosed configurations.